



OPEN

SUBJECT AREAS:
STRIATE CORTEX
RETINAReceived
29 July 2014Accepted
10 December 2014Published
13 January 2015Correspondence and
requests for materials
should be addressed to
Y.Y. (yangyp@ustc.
edu.cn)

The Topographical Arrangement of Cutoff Spatial Frequencies across Lower and Upper Visual Fields in Mouse V1

Xian Zhang¹, Xu An¹, Hanxiao Liu¹, Jing Peng¹, Shanshan Cai¹, Wei Wang², Da-Ting Lin³ & Yupeng Yang¹¹CAS Key Laboratory of Brain Function and Diseases, School of Life Sciences, University of Science and Technology of China, Hefei 230027, P.R. China, ²Institute of Neuroscience and State Key Laboratory of Neuroscience, Shanghai Institutes for Biological Sciences, Chinese Academy of Sciences, Shanghai 200031, P. R. China, ³Intramural Research Programme, National Institute on Drug Abuse, National Institutes of Health, Baltimore MD 21224.

The visual response to spatial frequency (SF), a characteristic of spatial structure across position in space, is of particular importance for animal survival. A natural challenge for rodents is to detect predators as early as possible while foraging. Whether neurons in mouse primary visual cortex (V1) are functionally organized to meet this challenge remains unclear. Combining intrinsic signal optical imaging and single-unit recording, we found that the cutoff SF was much greater for neurons whose receptive fields were located above the mouse. Specifically, we discovered that the cutoff SF increased in a gradient that was positively correlated with the elevation in the visual field. This organization was present at eye opening and persisted through adulthood. Dark rearing delayed the maturation of the cutoff SF globally, but had little impact on the topographical organization of the cutoff SF, suggesting that this regional distribution is innately determined. This form of cortical organization of different SFs may benefit the mouse for detection of airborne threats in the natural environment.

Mammals in their natural environments mainly rely on the visual system for foraging, hunting for prey and detecting attacks. To meet this demand, the central region of the retina in carnivores and primates contains an area with a high density of photoreceptors and closely packed ganglion cells (the area centralis in cats or fovea in primates). Consequently a large portion of the primary visual cortex (V1) is mapped to the portion of the visual field corresponding to this region^{1,2}, which exhibits higher visual acuity than that representing the peripheral visual fields. For rodents, food-seeking behaviour broadly occurs in the region of the lower visual field, and engages multiple sensory systems including olfaction, audition, and tactile sensation. To monitor the approach of predators, especially airborne predators, rodents have to rely mostly on visual information from the upper visual field. Given that the rod-dominated photoreceptors are evenly distributed across the retina³, mice were originally considered as having uniformly blurred vision across the visual field. However, recent behavioural studies show that the rodent maintains a constant surveillance of its upper visual field and is sensitive to objects appearing from that direction^{4,5}. Studies of the retina have also revealed that some types of the cones and retinal ganglion cells are distributed with a higher density in the ventral part of mouse retina^{6–8}, which views the upper visual field. Thus, an interesting question is whether and how the mouse visual system processes different visual information from the upper and lower visual fields, particularly at the cortical level.

The cutoff SF is one of the most important visual properties that quantify in a precise way the highest sinusoidal grating frequency resolvable by the visual system. Mammalian V1 is believed to be the most important stage in processing detailed vision^{9–11}. Recent electrophysiological studies^{12,13} reveal that V1 neurons in mice show clear selectivity for orientation and SF, similar to cats and monkeys. However, in contrast to the columnar organization of orientation and SF in the carnivore and primate^{14,15}, neurons with distinct visual feature selectivity in mouse V1 are reported to intermix in a “salt and pepper” manner as revealed by two-photon imaging¹⁶. Previous electrophysiological and imaging studies in rodents have focused on the peak but not the cutoff SF^{13,16}, although the latter is more closely related to grating acuity¹⁰. Thus, an open question is how the cutoff SF is organized in mouse V1. Furthermore, visual deprivation via dark rearing has little impact on the formation of ocular dominance and orientation preference in kittens¹⁷, but impairs the development of direction selectivity in ferrets¹⁸ and rodents¹⁹. It is also unclear whether visual experience has an impact on the formation of SF organization during postnatal brain development.

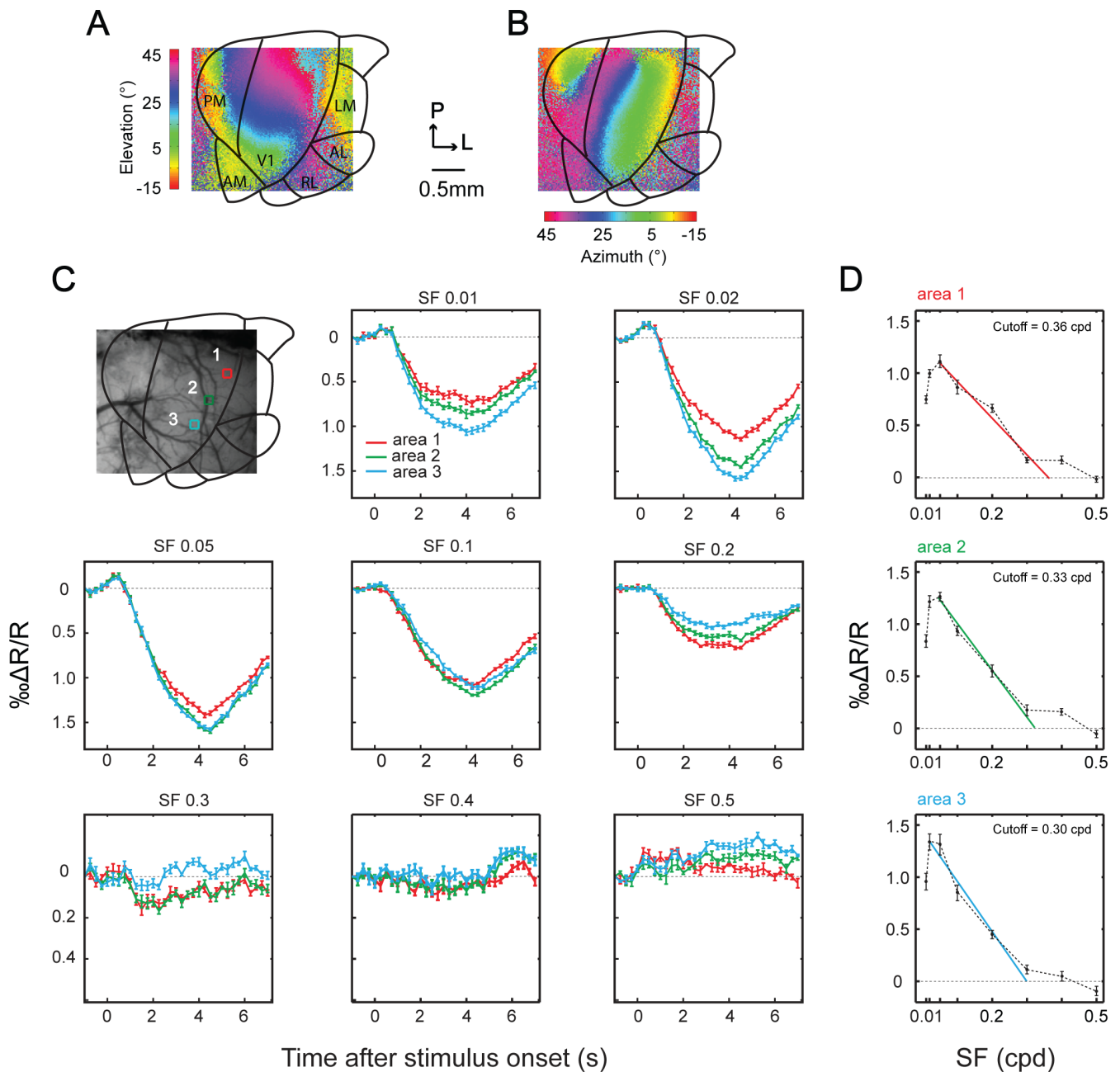


Figure 1 | Retinotopic maps and time courses of responses to different SFs. (A, B) Retinotopic maps of absolute isoelevation (A) and isoazimuth (B) respectively. A schema of mouse visual areas was applied to exclude extrastriate visual cortices. P: posterior; L: lateral; Scale bar: 0.5 mm (C) Time courses of averaged response strength ($\Delta R/R$) at different cortical regions (8×8 pixels) were evoked by different SF (in cycles per degree) stimuli. The locations of sampled areas indicated by red, green and blue frameworks, respectively, on the image of exposed cortical surface. Error bars represent s.e.m. (D) SF tuning curves to each stimulus SFs at different cortical areas using linear fittings (see Methods). Error bars represent standard deviation. P: posterior; L: lateral; Scale bar: 0.5 mm.

In this study, using intrinsic signal optical imaging and spherically corrected sinusoidal grating stimuli, we found an increasing gradient in the population responses of mouse V1 to stimulus SFs from the anterior to the posterior part. The imaging results were confirmed by subsequent single-unit recordings. To further investigate the development of this arrangement, and the effect of visual experience, we performed recordings of mice in both normal- and dark-reared conditions from eye opening to adulthood. We found that the cutoff SF of mice gradually matured during development and this process was delayed by deprivation of visual experience. However, the representation of cutoff SFs from lower to upper visual field was apparent a few days after eye opening and was maintained after dark rearing. Thus,

we speculate that the topographical organization of cutoff SFs across the visual field in mice is innate, and reflects the evolutionary benefit for mice in better detecting predation from above^{4,5,20}.

Results

Mouse V1 Has Higher Cutoff Spatial Frequencies in the Upper Visual Field. Population responses in mouse V1 were recorded using an intrinsic signal optical imaging approach. Spherically corrected sinusoidal gratings²¹ were applied to maintain SF and temporal frequency (TF) constant across the visual field. The retinotopic maps (Fig. 1A), which were generated with a drifting bar, were consistent with those in other studies^{21–23}. The areas activated in these images

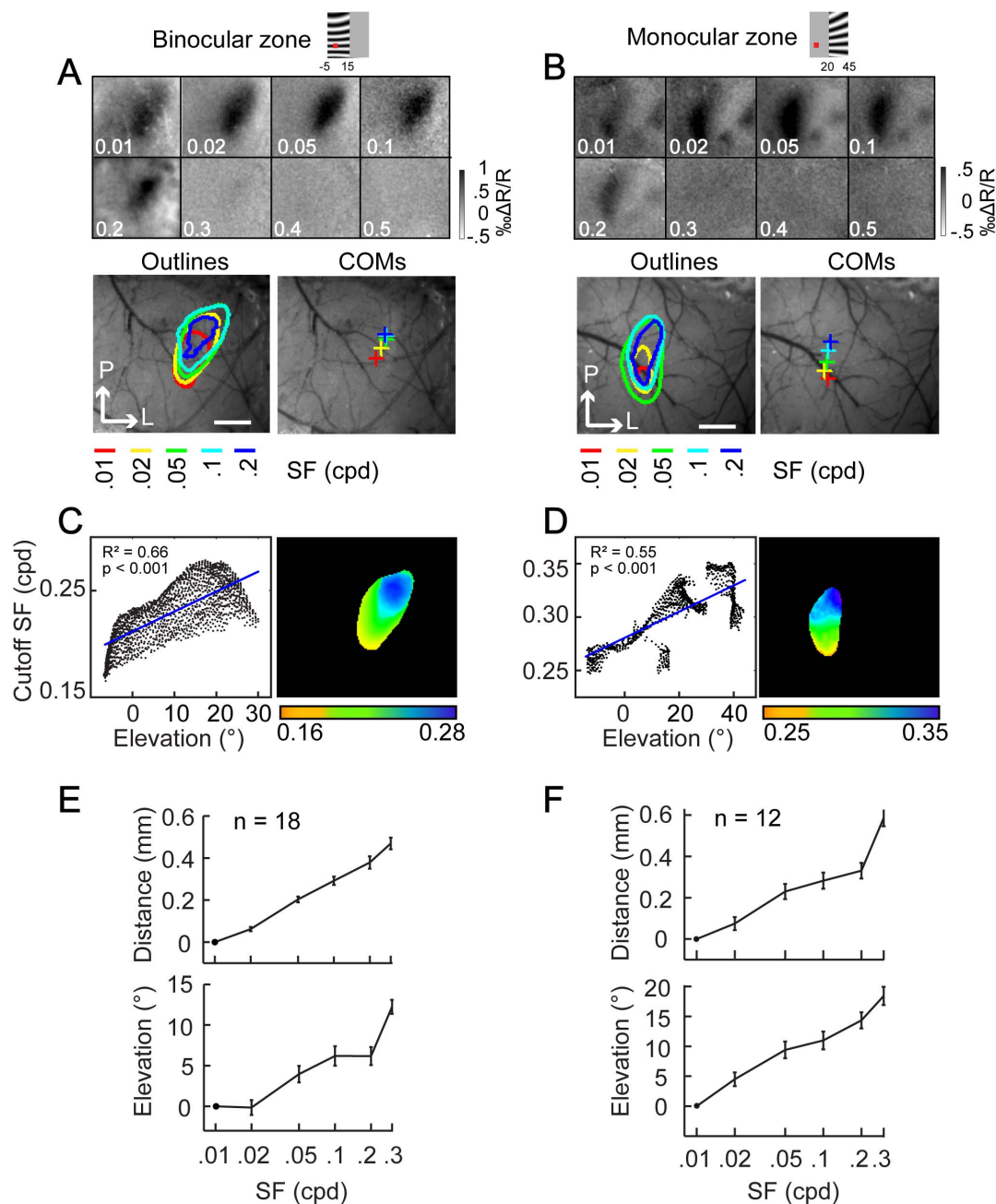


Figure 2 | The anteroposterior gradient distribution of SFs in both binocular and monocular zones. (A and B) Upper panel: Single-condition maps evoked by stimuli with different SFs. Lower panel: The outlines and COMs of different SF response modules are plotted together on the vasculature maps, respectively. P: posterior; L: lateral; Scale bar: 0.5 mm. (C and D) Correlation between the cutoff SF and elevation. (E and F) Upper panel: Δ dis; Lower panel: Δ ele. This shift in binocular zone was not significantly different from that in the monocular zone (Two-tailed *t* test, $p = 0.20$ and 0.42 for distance and elevation respectively). Error bar represents s.e.m.

include V1 and several extrastriate visual areas, including the anteromedial area, posteromedial area, and lateralmedial area²⁴. To exclude extrastriate response modules, a schema of mouse visual areas (Fig. 1A, 1B) was applied as previously described^{21,22,24}.

We first acquired maps of responses to a series of gratings of different SFs in adult mice. The maps of reflectance changes were averaged across presentations in each stimulus condition, and then subtracted and divided by the map obtained in the blank (pre-stimulus) condition, to form a single condition map (see Materials and Methods for detail). The signal amplitude ($\Delta R/R$) derived from the single condition map increased over 4–5 seconds after the stimulus onset (Fig. 1C). Each site in V1 exhibited clear responses to stimuli with SF below 0.4 cycles per degree (cpd). However, the response

strength differed from location to location depending on stimulus SFs (Fig. 1C). Typically, high SFs (>0.1 cpd) induced relatively larger responses at the region located in the posterior part of V1 (area 1, the red curve), whereas low SFs evoked stronger responses at the area located in the anterior part (area 3, the blue curve). We also plotted the SF tuning curves and determined the value of the cutoff SF for each cortical area (Fig. 1D). The cutoff SFs from anterior to posterior areas were 0.30, 0.33 and 0.36, respectively. Because the anterior and posterior parts of V1 represent the lower and upper visual fields (Fig. 1A)^{23,25}, these results indicated that neurons in mouse V1 corresponding to the upper vision are sensitive to high SFs.

The visual stimuli were displayed in binocular and monocular zones, respectively (Fig. 2A, 2B). Two examples show the single



condition maps in both areas. To determine the shift of population responses, the outline and the centre of mass (COM, Equation 1 in Methods) of each SF response area were calculated and plotted on the vasculature map (Fig. 2A, 2B). Although the SF response patches overlapped, they nevertheless shifted clearly towards the posterior part of V1 with the increase in SFs in both zones. We next constructed the colour-coded maps of the cutoff SFs on a pixel-by-pixel basis, which illustrated a clear correlation between cutoff SFs and elevation within V1 (Fig. 2C, 2D).

To quantify the shift of population responses from all of our experimental subjects, we computed the relative shift in distance (Δ_{dis}) and elevation (Δ_{ele}) (see methods). The cortical position and elevation of each COM were calculated and were found to shift in a SF-dependent manner (Fig. 2E, 2F). The average relative shift between the COMs (Equation 2 in Methods) of 0.01 cpd and 0.3 cpd in the binocular zone was 0.46 ± 0.05 mm (mean \pm s.e.m) in distance, which corresponded to 12.0 ± 1.7 degrees in elevation. A similar shift was observed in the monocular zone (0.58 ± 0.08 mm in distance and 18.4 ± 3.0 degrees in elevation).

It has been shown that receptive field size is positively correlated with azimuth in the mouse visual system^{12,26}, suggesting that the SF preference is negatively correlated with azimuth. We thus examined the shift of COMs in the azimuth-direction in 7 cases (Supplementary Fig. 1B). The average shift between COMs of 0.01 cpd and 0.3 cpd in the binocular zone was 6.3 ± 2.0 degrees in azimuth, which was significantly smaller than that in elevation (12.0 ± 1.7 degrees, Two-tailed *t* test, $p = 0.037$). Similarly in the monocular zone, the average shift between COMs of 0.01 cpd and 0.3 cpd in azimuth (2.2 ± 1.6 degrees) was also significantly smaller than that in elevation (18.4 ± 3.0 degrees, Two-tailed *t* test, $p = 0.0028$).

Though neurons in mouse V1 show orientation selectivity^{12,13}, no orientation preference maps were found in our optical imaging experiments, consistent with previous study²⁷. Nevertheless, to determine whether the orientation of the stimuli was critical to our observation, we performed experiments using grating stimuli with orthogonal orientation. Regardless of stimulus orientation, the outlines and COMs of SF maps shifted toward the posterior part of V1 with an increase in SF (Supplementary Fig. 2A, 2B, the monocular zone of an example animal), and the cutoff SF was positively correlated with elevation (Supplementary Fig. 2C). Finally, we did not observe any locally continued patchy organization of SFs, as shown in V1 of other species^{14,15}. Altogether, these population results indicate that there is a low to high gradient of cutoff SFs from anterior to posterior parts in mouse V1.

Electrophysiological Recordings Reveal Higher Cutoff SFs in the Upper Visual Field. The SF tuning properties of neurons in rodent V1 have been well documented in previous electrophysiological and two-photon calcium imaging studies^{12,13,21,22}. However, the relationship between the cutoff SF and elevation has not been examined. To validate the population findings, we performed single-unit recordings (Fig. 3A and 3B) from neurons in the representation of different elevations of V1, guided by the optical imaging results and the vasculature pattern (see examples of SF tuning in Fig. 3D). The raw signal was offline sorted into single unit as previously described²⁸. Overall, the mean peak and cutoff SFs across our cell populations (119 cells in 10 adult mice) were 0.046 ± 0.002 cpd and 0.31 ± 0.01 cpd, respectively (Fig. 3I), consistent with previous single-unit recording and brain imaging results in V1^{12,13,21,22}. We also found a significant positive correlation between the peak and cutoff SFs (Fig. 3J). However, the distribution of the cutoff SF had a span about five-fold larger than that of the peak SF (Fig. 3I), indicating that a structured SF map might be more observable with the cutoff SF than that with the peak SF. In agreement with the optical imaging results, the cutoff SF was significantly correlated with elevation (Fig. 3E). Furthermore, neurons representing the binocular

visual field seemed to possess high cutoff SFs (Fig. 3F), confirming the central-lateral shifts of COMs by optical imaging (Supplementary Fig. 2). However, there was no significant correlation between the peak SF and elevation (Fig. 3G) or azimuth (Fig. 3H).

We built a simple model to help us understand whether the single-unit findings were consistent with the population responses measured by intrinsic optical signals. In this model, each pixel in the response map represented a neuron with a random peak and bandwidth of SF that followed the distribution from both our and previous single-unit recording data¹². If the peak SFs of all pixels were randomly distributed (100% randomness), all COMs of the responses to different SFs should remain in the center of the simulate area (Fig. 4A). On the other hand, if the peak SFs of pixels were linearly increased along elevation direction (0% randomness), the activated patches and the COMs of higher SFs would clearly shift towards higher elevation (Fig. 4B). If the coordinates of only some pixels were randomly shuffled, the amplitudes of the shifts would diminish (Fig. 4C, 75% random). Indeed, the shift amplitude was negatively correlated with that of randomness in a linear way (Fig. 4D). The average elevation change between COMs of 0.01 and 0.1 cpd normalized to the whole elevation range in our optical imaging experiment was 11% in the binocular zone, similar to 75% randomness condition in the model. We thus randomly selected 100 neurons out from this model with condition of 75% randomness. We found that the distributions of both the peak and cutoff SF resembled our single-unit recording results (Fig. 3I, 4E and 4F).

The Impact of Visual Experience on the Formation of SF Organization. To examine how the topographical organization of SFs evolves during the postnatal development, we performed optical imaging experiments at different ages. Three groups of mice were studied: around the time of eye opening (P13–16, $n = 11$), at the beginning of the critical period (P21–24, $n = 6$), and at the time when the grating acuity was well developed (P28–32, $n = 7$)²⁹. The cutoff SFs of mice increased during development (Fig. 5A), similar to that observed in previous behavioural experiments³⁰. However, the outlines and COMs of SF modules of juvenile mice were apparent just 1–3 days after eye opening and showed a similar anteroposterior distribution of SF in both binocular (Fig. 5C) and monocular (Fig. S3A) zones. Thus, similar with adult mice, young mice possessed the globally topographical organization of cutoff SFs. Interestingly, the shift in elevation of COMs in young groups tended to be larger than that in the adult group (Fig. 5D and S3B). This is because young mice have relatively lower cutoff SFs than adult ones. The cortical magnification factor, which is positively correlated with visual acuity in human³¹, was also smaller in young mice than that in adult ones (Fig. 5B).

Early visual experience is critical to the normal postnatal development and maturation of many visual properties^{17,18,32}. To further study whether the topographical arrangement of SFs was inherent, we dark reared 11 mice from birth and performed intrinsic signal optical imaging at different ages. Because it was very difficult to obtain reproducible signals in dark-reared mice before weaning, we chose three ages: P21–24 ($n = 4$), P28–34 ($n = 4$), and P39–42 ($n = 3$). The dark-reared groups showed significantly lower cutoff SFs when compared with that of control groups at the same age (P21 group, $p = 0.042$; P28 group, $p = 0.031$; Two-tailed *t* test, Fig. 5A), suggesting that the visual experience is required for the maturation of cutoff SFs³³. Nevertheless, similar to the results in the normally-reared group, the responsive areas in dark-reared mice also shifted gradually from anterior to posterior parts of V1 when SF was increased (binocular zone, Fig. 5E and 5F; monocular zone, Fig. S3C and S3D), suggesting the topographical distribution of SFs in V1 is an intrinsic property.

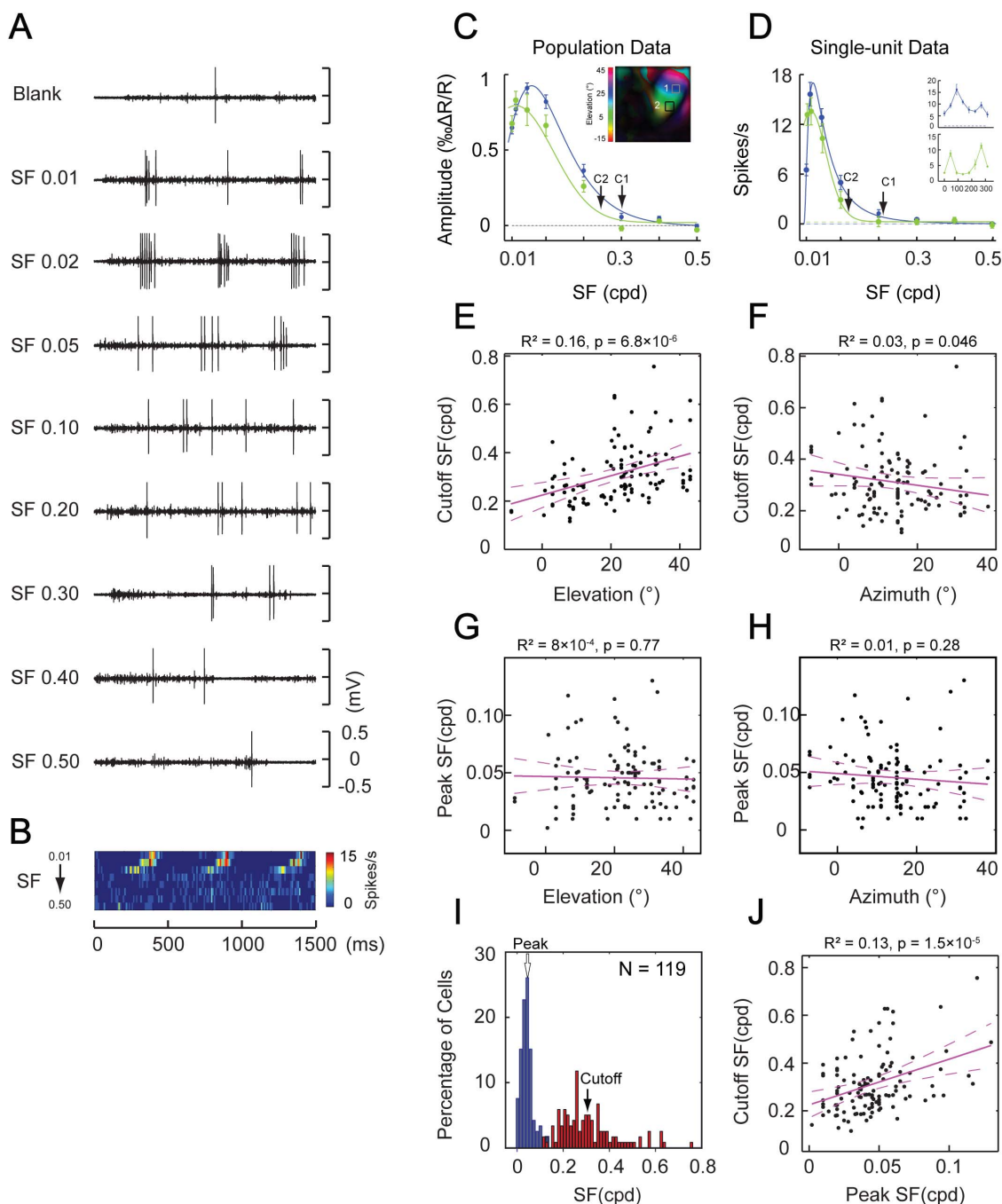


Figure 3 | The anteroposterior distribution of cutoff SFs at the single-cell level. (A) Neural spike trains to each stimulus grating displayed for 3 cycles. (B) Heat map of 150 ms of average firings from 10 repetitions. (C) SF tuning curves in different elevations from population responses. Hues in the retinotopic map represented elevations and brightness represents responsive amplitude. The peak and cutoff SFs for area 2 were 0.02 and 0.25 cpd respectively. C1 and C2 mark the cutoff SF of each area in tuning curves. Error bar represents standard deviation. (D) The SF tunings of two example neurons in the corresponding upper (Cutoff SF = 0.21 cpd) and lower (Cutoff SF = 0.12 cpd) visual fields. The upper right panel shows direction selectivity of two cells. C1 and C2 mark the cutoff SF of each cell in tuning curves. Error bar represents s.e.m. (E) The correlation between the cutoff SF and elevation. The dashed pink lines represent the 95% confidence interval. (F) The correlation between the cutoff SF and azimuth. (G) The correlation between the peak SF and elevation. (H) The correlation between the peak SF and azimuth. (I) The histogram distributions of the peak (blue) and cutoff (red) SFs of all neurons ($N = 119$). The white and black arrows indicate the mean peak and cutoff SFs. (J) The correlation between the peak and cutoff SF.

Discussion

Despite the restricted visual ability, contrast sensitivity, and the relatively small size of V1²⁷, the mouse visual system has become one of the most popular model systems for studying neural development and circuit mechanisms³⁴. Unlike carnivore and primate V1, where neurons with the high spatial frequency preferences reside in a spe-

cific cortical region corresponding to the area centralis or fovea^{35,36}, neurons in mouse V1 with higher cutoff SFs tend to be situated in the posterior part of V1 that represents the upper visual field. Furthermore, different from the orientation preferences that are organized in a “salt and pepper” manner in mouse V1, the cutoff SFs showed a progression from anterior to posterior across V1. This

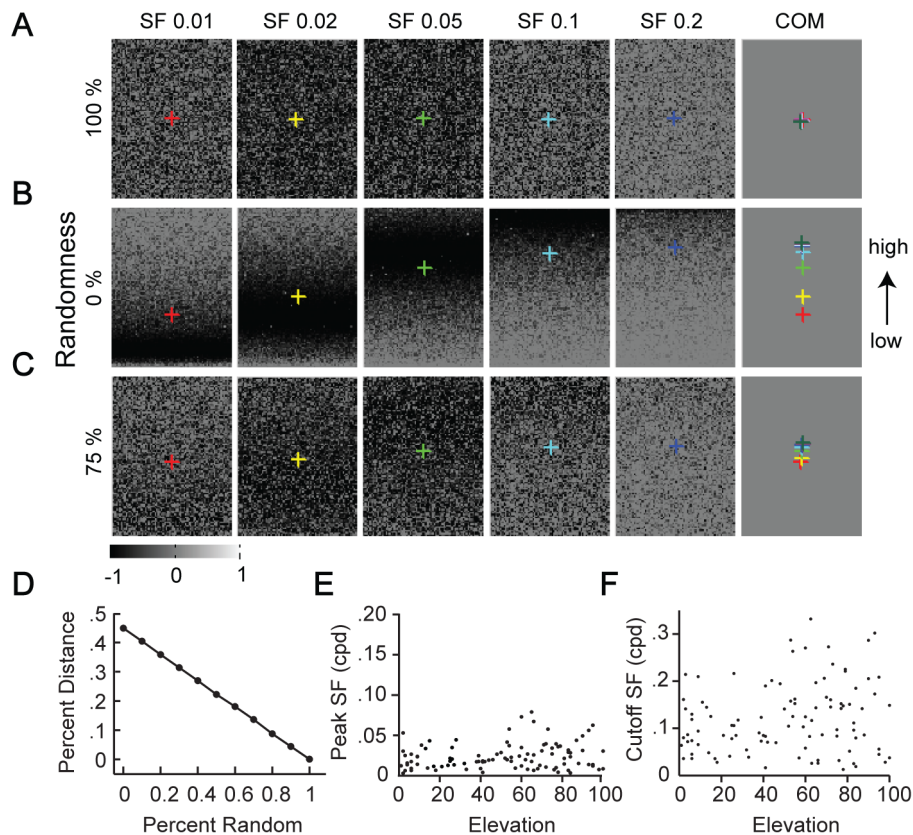


Figure 4 | Model simulation for the SF organization. (A, B, C) The modeled distribution of population responses. Neurons with different SF preference were distributed randomly (A), regularly under 0% randomness condition (B), or under 75% randomness condition (C) along elevation. In all images, black indicates the maximum response while grey indicates no response. The crosses with different colours represent the locations of COMs. The bottom of the image corresponds to low elevation as indicated by the black arrow on the right. (D) The relationship between the randomness of neurons and the percentage of shift in the distance (between COM of 0.01 and 0.1 cpd) versus whole length of the area. The simulation was repeated ten times. The s.e.m was too small to be shown. (E and F) The distribution of the peak and cut-off SFs of 100 randomly selected model neurons from the simulation condition when 75% neurons have random peak SFs.

gradient distribution of cutoff SFs was apparent soon after eye opening and was present even without visual experience, indicating that this property is innate. Given the behavioural evidence suggesting that rodents show better sensitivities to overhead visual information^{4,5}, this arrangement of cutoff SFs in mouse V1 is consistent with an adaptation to the natural environment for survival.

Detection of predators should benefit from high spatial resolution⁷ and the primary visual cortex is a crucial brain region for processing high visual acuity^{9,11}. Developing higher cutoff SFs at higher elevations enables the mouse to detect objects signifying danger at a greater distance, improving behavioural preparations to flee before an attack occurs^{7,20}. For example, at the upper most part of the visual field, mice with a cutoff SF of 0.4 cpd can detect a black object subtending 1.25° of visual angle. This is consistent with a bird at a distance of about 46 wing spans. However, with a cutoff SF of 0.1 cpd, the mouse can only see a bird at a distance of 12 wing spans, which might be too late if the bird is rapidly approaching⁷. In addition, objects in the upper visual field, tend to be far away, whereas in the lower visual field, objects of interest tend to be closer because distant objects are occluded by nearer ones. Events occurring on the ground can also be detected by the collaboration of multiple sensory systems, thus vision becomes less crucial. Hence, the gradient distribution of cutoff SFs we observed is consistent with an adaptation to this natural requirement.

The retinocollicular pathway in mice has been hypothesised to mediate rapid defensive behaviours to looming stimuli⁴. The superficial layer in rodent superior colliculus receives direct cortical inputs from the primary visual cortex^{37,38}, especially those visual inputs

conveying low SF signals³⁷. Neurons in V1 can also process the visual information rapidly, within 0.2 seconds, regardless of the SF¹². Thus, mouse V1 may also modulate or contribute to those vision-driven responses. A recent study has revealed V1 modulates the magnitude of looming-evoked responses in superior colliculus of awake mice³⁹. Therefore, V1 would be expected to be particularly important for identifying potential threats among the large number of visual objects¹¹, or to increase the overall alertness of the animal before potential attacks are detected by other mechanisms like “looming detectors”⁷⁴.

The front end of the visual system has also evolved over time to fit the animal’s own living environments. The distribution of rods across mouse retina is relatively uniform³. However, the cones in mouse retina exhibit remarkable regional variation. The ultraviolet sensitive S-cones are expressed in the ventral retina^{40,41}, enabling the mouse to have a better contrast sensitivity towards the sky⁸. Meanwhile, experiments in the retinal ganglion cells (RGCs) have revealed that the RGCs are distributed non-uniformly. The melanopsin-positive RGCs have a dorsal to ventral gradient distribution⁶. The “w3” population of the RGCs with the smallest receptive field, are sensitive to local motion within the receptive field and have been proposed to serve as alarm neurons for overhead predators⁷. Alpha cells, one kind of RGC, exhibits dramatic variation in size and cell density along the nasal to temporal retinal axis²⁶. This gradient distribution may benefit mice to have high spatial representation of the binocular field. Rat retina has the highest RGC density located temporal and just above the optic disc⁴², which is corresponding to approximately 60° temporally and 35° above the horizontal^{43,44}.

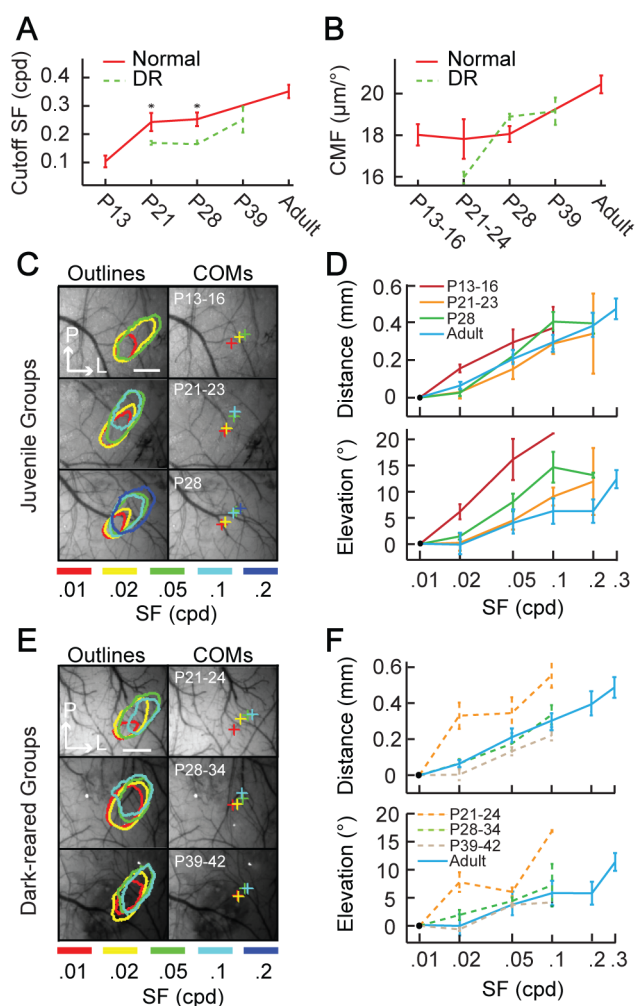


Figure 5 | The topographical organization of SFs in binocular zone of juvenile and dark-reared mice. (A) The development of grating acuity in normal and dark-reared animals. Asterisks indicate significant differences ($p < 0.05$) between the two groups at the same ages (normal, $n = 24$; dark reared, $n = 11$). (B) The development of cortical magnification factor in normal and dark-reared mice (normal, $n = 24$; dark reared, $n = 11$). The CMF increased gradually with postnatal days in both juvenile and DR groups, but the CMF was not significant different between two groups at the same ages (Two-tailed t test, P21: $P = 0.13$; P28: $P = 0.15$). (C) Outlines and COMs of domains responding to SFs indicated in the binocular zone of different postnatal stages. P: posterior; L: lateral; Scale bar: 0.5 mm. (D) Shifts of COMs with cortical distance and elevation in the binocular zone at different ages. Error bar represents s.e.m. (E) The outlines and COMs of SF domains in the binocular zone of dark-reared groups at different ages. P: posterior; L: lateral; Scale bar: 0.5 mm. (F) Shifts of COMs with cortical distance and elevation in dark-reared animals at different ages. Error bar represents s.e.m. CMF: Cortical magnification factor.

These findings are in line with our observation of an increasing gradient in the cutoff SF from lower and lateral to upper and central visual fields.

Two forms of spatial visual acuity have been characterized in primates: Vernier and grating acuity^{45,46}. Vernier acuity measures the sensitivity to the relative position of pattern elements, which may surpass the spatial resolving power of cells in retina and hold a precision up to 10 times better than may be expected⁴⁷ (known as hyperacuity). Experiments in monkey retina show that magnocellular ganglion cell responses are closely linked to psychophysically measured hyperacuity⁴⁸, and the magnocellular pathway is known

to have substantial spatial non-linearity⁴⁹. This is consistent with modelling study showing that nonlinear processes better reproduction of the responses to spatial structure⁵⁰. Meanwhile, the spatial contrast sensitivity of neurons characterized by sinusoidal grating is correlated with grating acuity which is a measure of the finest resolvable detail⁴⁵. Animals with higher grating acuity tend to have higher SF sensitivity⁵¹. For example, cats and monkeys have higher SF selectivity than mice. Previous studies in rodent have not focused on Vernier acuity^{9,11} or investigated nonlinear integration mechanisms. Thus, how acuity precisely correlates with cutoff SFs in rodents needs further investigation.

Though the organization for SF exists in many species^{14,15}, whether its developmental emergence depends on endogenous or experience-dependent mechanisms was previously unknown. Visual experience has been shown to have an impact on the maturation of orientation selectivity in mouse⁵² and direction selectivity in ferret V1^{18,32} but not in mouse V1¹⁹. A recent study in naive mice indicates that the formation of the fine structure of the spatial receptive field is experience-independent⁵³. Furthermore, in carnivore and primate V1, orientation columns emerge independent of patterned visual experience^{17,54}. Our current findings and previous behavioral experiment³³ show that the refinement of visual responses to gratings of different SFs is delayed by visual deprivation. However, the anteroposterior tendency of cutoff SFs in mouse V1 was apparent at different ages and was also preserved during dark rearing. Therefore, our data indicate that the SF segregation in mice arises from endogenous activity.

Several possible reasons may contribute to previous work having failed to find a spatial distribution when using the peak SF. First, mouse V1 neurons have a limited span of the peak SF distribution, about 5 times less than that of the cutoff SF distribution (Fig. 3C). Second, two-photon imaging only examines a cortical region representing a limited range of elevations^{16,21,22}. Third, it is crucial that sinusoidal gratings are spherically corrected when presented at large eccentricity, especially for popular recording methods such as two-photon calcium imaging, intrinsic signal optical imaging, and multi-unit recordings. The actual SF at the site with an eccentricity of 45° would be underestimated by about 30% without spherical correction. Lastly, in considering the high randomness of SF distribution as estimated by our model simulations, it would be very difficult to reveal the distribution rule when using the peak SF as in previous studies.

To date, visual functions in the mouse early visual system are still poorly understood. Different to carnivores and primates, rodents have two pathways that are presumably equally important in visual information processing: the retina to superior colliculus pathway and the retina to V1 pathway. The looming response is proposed to rely on the retina-superior colliculus pathway⁴, while the visual cortex with high spatial resolution is needed for object recognition¹⁰. Approaches using genetic and optogenetic manipulations in the behaving mouse³⁴ may be applied to elucidate other differences in visual information processing between upper and lower visual field, and to characterize the crosstalk between colliculus and visual cortices in visually driven behaviours.

Methods

All surgical and experiments were conducted in accordance with protocols approved by the Animal Care and Use Committee at the University of Science and Technology of China.

Surgical procedure. Adult C57BL/6 mice ($n = 23$) between 2–5 months, juvenile mice between P13–P32 ($n = 24$) of normal development and P21–P42 ($n = 11$) of dark rearing were used in our experiments. All subjects were initially anaesthetized with isoflurane (2–3%) or intraperitoneal injection of Ketamine (0.1 mg/g) and Xylazine (0.01 mg/g) mixture⁵⁵, and then were maintained by isoflurane (0.5–1%). Animals were fixed in a customized stereotaxic apparatus mounted on a vibration isolation table. The core temperature were maintained at 37.5°C by a feedback controlled heating pad. The scalp was trimmed off and lidocaine solution was dripped in the wound occasionally to reduce the pain. The skull was then carefully thinned by



micro-drill, and a few drops of silicone oil were applied to the bone to make it transparent enough for intrinsic signal optical imaging.

Visual stimulation. Visual stimuli were created by MATLAB (Mathworks, Massachusetts, USA) using the Psychophysics Toolbox^{56,57} and displayed on a gamma-corrected large LCD monitor with mean luminance about 32 cd/m². The monitor was placed 24 cm in front of the animal. The visual monitor in this experiment is flat. However, eccentricity of visual fields is often defined in a spherical parameter. Therefore, when stimuli are presented at a higher eccentricity (e.g. 45°), such distortion would make actual SF underestimated (30%) without the spherical correction. Hence, in this experiment, spherically corrected sinusoidal gratings were needed to maintain SF and temporal frequency (TF) constant across the visual field (upper panel in Fig. 2A and 2B)²¹. The sinusoidal gratings were displayed on monocular visual field (+20° to +45° horizontal by -15° to +45° vertical) or binocular visual field (-5° to +15° horizontal by -15° to +45° vertical). For drifting grating experiments, the stimuli were displayed for 4 s. A grey screen was shown during the prestimulus baseline period (1 s) and between trials (7 s). For both intrinsic signal optical imaging and extracellular recording, we employed a set of sinusoidal grating stimuli with SFs of 0.01, 0.02, 0.05, 0.1, 0.2, 0.3, 0.4, 0.5 cpd and temporal frequency of 2 Hz. For mapping retinotopy, a white bar was drifted at two opposite directions along each cardinal axis for 10 minutes periodically at 0.1 Hz as previously described²³.

Intrinsic Signal Optical Imaging and Data Analysis. Intrinsic signal optical imaging was performed in mouse visual cortex using the method as described previously^{58,59}. The recorded area was illuminated with green light of 550 nm to obtain a brain vasculature map and red light of 720 nm to acquire evoked responses. Images were captured using a Dalsa Pantera 1M60 CCD camera. Images were obtained with a resolution of ~17 μm/pixel. Retinotopic maps were computed as previously described²³. Fourier analysis was used to extract two matrices pixel by pixel: one for response strength at stimulus frequency and the other was a phase matrix representing stimulus eccentricity. The iso-azimuth and -elevation contours were plotted together to reveal the full retinotopic map (Fig. 1A and 1B). The cortical magnification factors in azimuth and elevation axes were determined by calculating the mean distance between two adjacent nodes in the retinotopic grids. Frames taken after the stimulus onset for 2–6 s were averaged and then a blank frame (the average response to the 1 second interval prior to the stimulus onset) was subtracted and divided to generate a single-condition map of reflectance change (ΔR/R). To avoid signal distortion, all images were smoothed (kernel of 2 pixels or 34 μm in radius) by circular averaging filter. All filtered ΔR/R maps acquired from the same stimulus condition across 32 trials were averaged to obtain an average single condition map. To reveal SF responsive patches, we smoothed all images first and then performed a two-tailed t test between single-condition and blank maps across 32 trials. Only pixels with P value less than 0.05 were regarded as responsive and were selected for further analysis. The contour was then defined automatically by “bwperim” function in MATLAB. The value of connectivity was 8. To exclude extrastriate areas, we masked the single condition map by the schema previously depicted^{21,22,24}. The centre of mass of each responsive module for different SFs was calculated by:

$$[COM_x, COM_y] = \left[\frac{1}{n * r} \sum_{i=1}^n x_i * r_i, \frac{1}{n * r} \sum_{i=1}^n y_i * r_i \right] \quad (1)$$

Where x and y are coordinate values, r_i is the response amplitude in the corresponding location, r is the mean response amplitude. We also calculated the relative shifts in distance and elevation of all COMs and COM 0.01. The distance between each COM and COM 0.01 was calculated by:

$$\Delta dist(COM, COM0.01) = \sqrt{\Delta x^2 + \Delta y^2} \quad (2)$$

The difference of elevation between each COM and COM 0.01 was calculated by: Δele = elevation(COM) - elevation(0.01). Consistent with previous study⁹, the cutoff SF for each pixel was computed by linear fitting (See examples in Fig. 1D). The SFs for this fitting are from a SF evoked maximum response intensity to a SF evoked a response value less than 2 SD. To generate the colour-coded cutoff SF map, pixels were colour coded according to their cutoff SFs. The cutoff SF of the mouse in different ages was calculated by linear fitting using intrinsic signal optical imaging results.

Electrophysiological Recording and Data Analysis. In 10 out of 23 adult animals, after intrinsic signal optical imaging, we performed extracellular recording to collect neuronal firing with high signal to ratio (Fig. 3A) as described recording in cat in our recent study⁶⁰. Briefly, the electrode was advanced vertically via a hydraulic micromanipulator (Narishige, Tokyo, Japan) and was inserted in different sites of the striate visual cortex (Figs 3E and 3F) to record neurons with receptive fields in different elevations. Raw neural signals were amplified and bandpass filtered from 300 to 3000 HZ using the amplifier (Dagan, Minnesota, USA), and then digitized using a data acquisition board (National Instruments, Texas, USA) controlled by customized programmes operated in the MATLAB environments. The receptive field size of neuron was determined by measuring the major and minor axes using a hand-held bar. Stimuli were displayed in a circular window covering the receptive field of the cell. Next, each neuron was tested for tuning to orientation, spatial frequency and sometimes temporal frequency. Every different tuning function was acquired in a

separate block of random interval trials. For spatial frequency tuning, a stimulus moving in orthogonal directions with different SFs was shown in a circular window covering the receptive field for 3 cycles and repeated 10 times. The inter-stimulus interval was 3 s. The firings were offline sorted into single units as previously described²⁸. The offline sorting programme was provided by Dr. Quian Quiroga in his website. The response of neurons for each trial was calculated using the mean firing rate. Then, the SF tuning curve was fitted with a log Gaussian function¹²:

$$y = B + A * e^{-\frac{1}{2s^2} * \log\left(\frac{x+o}{p}\right)^2} \quad (3)$$

Where B is baseline firing rate, A is response amplitude, s is SD, o is log offset, p is peak SF, and e is the Euler's constant. The fitting was performed in MATLAB using the curve fitting toolbox. The cutoff SF were defined by locating the highest SF where the fitted response level dropped to 10% of maximum response¹², which is similar with the rate of spontaneous activity⁶¹.

In general, we used linear regression analyses to examine the correlation between two variables. The confidence interval of the linear fit was assessed using ‘predint’ function in MATLAB. Data represent mean ± s.e.m or mean + SD.

Model Simulation. We simplified the superficial layers of the mouse primary visual cortex as filled with 100 × 75 neurons according to the intrinsic signal optical imaging results which showed that the cortex exhibited a larger extent along the elevation (Fig. 2E and 2F). The SF tunings of the neurons in our model followed a Gaussian function as described above. We built a large pool of neurons (75000) with the peak SF and SF bandwidth distributions adopted from previous electrophysiological recording study (Figs 6A and 6C in Niell and Stryker, 2008). The maximum peak SF was limited to 0.13 cpd to match our single-unit results (Fig. 3K) and previous findings^{12,13}. The cutoff SF of the neurons was defined as that at which 10% of the maximum response was elicited. We selected the 100 × 75 neurons randomly from the neuronal pool with cut-off SFs less than 0.8 cpd to match our single-unit results (Fig. 3K) and previous study¹². We arranged the neurons to follow a strict sequence that the peak SFs of the neurons increased with elevation. We also added randomness to the sequence by selecting some neurons and reorganizing their relative location randomly, so that 100% randomness meant all the neurons were randomly distributed and 75% randomness indicated that 25% neurons still followed the strict sequence while the other 75% neurons followed a random order. Responses from these neurons to stimuli with different SFs as used in optical imaging experiments were calculated and diagrammed (Figs 4A–C). The COMs of the responses were computed as in intrinsic signal analysis.

- Blasdel, G. & Campbell, D. Functional retinotopy of monkey visual cortex. *J. Neurosci.* **21**, 8286–8301 (2001).
- Tusa, R. J., Palmer, L. A. & Rosenquist, A. C. The retinotopic organization of area 17 (striate cortex) in the cat. *J. Comp. Neurol.* **177**, 213–235 (1978).
- Jeon, C. J., Strettoi, E. & Masland, R. H. The major cell populations of the mouse retina. *J. Neurosci.* **18**, 8936–8946 (1998).
- Yilmaz, M. & Meister, M. Rapid innate defensive responses of mice to looming visual stimuli. *Curr. Biol.* **23**, 2011–2015 (2013).
- Wallace, D. J. *et al.* Rats maintain an overhead binocular field at the expense of constant fusion. *Nature* **498**, 65–69 (2013).
- Hughes, S., Watson, T. S., Foster, R. G., Peirson, S. N. & Hankins, M. W. Nonuniform distribution and spectral tuning of photosensitive retinal ganglion cells of the mouse retina. *Curr. Biol.* **23**, 1696–1701 (2013).
- Zhang, Y., Kim, I. J., Sanes, J. R. & Meister, M. The most numerous ganglion cell type of the mouse retina is a selective feature detector. *Proc. Natl. Acad. Sci. USA* **109**, E2391–E2398 (2012).
- Applebury, M. L. *et al.* The murine cone photoreceptor: a single cone type expresses both S and M opsins with retinal spatial patterning. *Neuron* **27**, 513–523 (2000).
- Heimel, J. A., Hartman, R. J., Hermans, J. M. & Levelt, C. N. Screening mouse vision with intrinsic signal optical imaging. *Eur. J. Neurosci.* **25**, 795–804 (2007).
- Prusky, G. T. & Douglas, R. M. Developmental plasticity of mouse visual acuity. *Eur. J. Neurosci.* **17**, 167–173 (2003).
- Prusky, G. T. & Douglas, R. M. Characterization of mouse cortical spatial vision. *Vision Res.* **44**, 3411–3418 (2004).
- Gao, E., DeAngelis, G. C. & Burkhalter, A. Parallel input channels to mouse primary visual cortex. *J. Neurosci.* **30**, 5912–5926 (2010).
- Niell, C. M. & Stryker, M. P. Highly selective receptive fields in mouse visual cortex. *J. Neurosci.* **28**, 7520–7536 (2008).
- Nauhaus, I., Nielsen, K. J., Disney, A. A. & Callaway, E. M. Orthogonal micro-organization of orientation and spatial frequency in primate primary visual cortex. *Nat. Neurosci.* **15**, 1683–1690 (2012).
- Issa, N. P., Trepel, C. & Stryker, M. P. Spatial frequency maps in cat visual cortex. *J. Neurosci.* **20**, 8504–8514 (2000).
- Glickfeld, L. L., Andermann, M. L., Bonin, V. & Reid, R. C. Cortico-cortical projections in mouse visual cortex are functionally target specific. *Nat. Neurosci.* **16**, 219–226 (2013).
- Crair, M. C., Gillespie, D. C. & Stryker, M. P. The role of visual experience in the development of columns in cat visual cortex. *Science* **279**, 566–570 (1998).



18. Li, Y., Van Hooser, S. D., Mazurek, M., White, L. E. & Fitzpatrick, D. Experience with moving visual stimuli drives the early development of cortical direction selectivity. *Nature* **456**, 952–956 (2008).
19. Rochefort, N. L. *et al.* Development of direction selectivity in mouse cortical neurons. *Neuron* **71**, 425–432 (2011).
20. Morris, P. Rats in the Diet of the Barn Owl (*Tyto-Alba*). *J. Zool.* **189**, 540–545 (1979).
21. Marshel, J. H., Garrett, M. E., Nauhaus, I. & Callaway, E. M. Functional specialization of seven mouse visual cortical areas. *Neuron* **72**, 1040–1054 (2011).
22. Andermann, M. L., Kerlin, A. M., Roumis, D. K., Glickfeld, L. L. & Reid, R. C. Functional specialization of mouse higher visual cortical areas. *Neuron* **72**, 1025–1039 (2011).
23. Kalatsky, V. A. & Stryker, M. P. New paradigm for optical imaging: temporally encoded maps of intrinsic signal. *Neuron* **38**, 529–545 (2003).
24. Wang, Q. X. & Burkhalter, A. Area map of mouse visual cortex. *J. Comp. Neurol.* **502**, 339–357 (2007).
25. Schuett, S., Bonhoeffer, T. & Hubener, M. Mapping retinotopic structure in mouse visual cortex with optical imaging. *J. Neurosci.* **22**, 6549–6559 (2002).
26. Bleckert, A., Schwartz, G. W., Turner, M. H., Rieke, F. & Wong, R. O. Visual space is represented by nonmatching topographies of distinct mouse retinal ganglion cell types. *Curr. Biol.* **24**, 310–315 (2014).
27. Van Hooser, S. D., Heimel, J. A., Chung, S., Nelson, S. B. & Toth, L. J. Orientation selectivity without orientation maps in visual cortex of a highly visual mammal. *J. Neurosci.* **25**, 19–28 (2005).
28. Quiroga, R. Q., Nadasdy, Z. & Ben-Shaul, Y. Unsupervised spike detection and sorting with wavelets and superparamagnetic clustering. *Neural Comput.* **16**, 1661–1687 (2004).
29. Smith, S. L. & Trachtenberg, J. T. Experience-dependent binocular competition in the visual cortex begins at eye opening. *Nat. Neurosci.* **10**, 370–375 (2007).
30. Prusky, G. T., Alam, N. M., Beekman, S. & Douglas, R. M. Rapid quantification of adult and developing mouse spatial vision using a virtual optomotor system. *Inves. Ophthalmol. Vis. Sci.* **45**, 4611–4616 (2004).
31. Cowey, A. & Rolls, E. T. Human cortical magnification factor and its relation to visual acuity. *Exp. Brain Res.* **21**, 447–454 (1974).
32. Li, Y., Fitzpatrick, D. & White, L. E. The development of direction selectivity in ferret visual cortex requires early visual experience. *Nat. Neurosci.* **9**, 676–681 (2006).
33. Bartoletti, A., Medini, P., Berardi, N. & Maffei, L. Environmental enrichment prevents effects of dark-rearing in the rat visual cortex. *Nat. Neurosci.* **7**, 215–216 (2004).
34. Luo, L., Callaway, E. M. & Svoboda, K. Genetic dissection of neural circuits. *Neuron* **57**, 634–660 (2008).
35. Rapaport, D. H. & Stone, J. The area centralis of the retina in the cat and other mammals: focal point for function and development of the visual system. *Neuroscience* **11**, 289–301 (1984).
36. Hendrickson, A. & Kupfer, C. The histogenesis of the fovea in the macaque monkey. *Inves. Ophthalmol. Vis. Sci.* **15**, 746–756 (1976).
37. Wang, L., Sarnaik, R., Rangarajan, K., Liu, X. & Cang, J. Visual receptive field properties of neurons in the superficial superior colliculus of the mouse. *J. Neurosci.* **30**, 16573–16584 (2010).
38. Triplett, J. W. *et al.* Retinal input instructs alignment of visual topographic maps. *Cell* **139**, 175–185 (2009).
39. Zhao, X., Liu, M. & Cang, J. Visual Cortex Modulates the Magnitude but Not the Selectivity of Looming-Evoked Responses in the Superior Colliculus of Awake Mice. *Neuron* **84**, 202–213 (2014).
40. Haverkamp, S. *et al.* The primordial, blue-cone color system of the mouse retina. *J. Neurosci.* **25**, 5438–5445 (2005).
41. Szel, A., Rohlich, P., Mieziewska, K., Aguirre, G. & Vanvee, T. Spatial and Temporal Differences between the Expression of Short-Wave and Middle-Wave Sensitive Cone Pigments in the Mouse Retina - a Developmental-Study. *J. Comp. Neurol.* **331**, 564–577 (1993).
42. Fukuda, Y. A three-group classification of rat retinal ganglion cells: histological and physiological studies. *Brain Res.* **119**, 327–334 (1977).
43. Hughes, A. A schematic eye for the rat. *Vision Res.* **19**, 569–588 (1979).
44. Drager, U. C. Observations on monocular deprivation in mice. *J. Neurophysiol.* **41**, 28–42 (1978).
45. Skoczinski, A. M. & Norcia, A. M. Development of VEP Vernier acuity and grating acuity in human infants. *Inves. Ophthalmol. Vis. Sci.* **40**, 2411–2417 (1999).
46. Kiorpes, L. Development of vernier acuity and grating acuity in normally reared monkeys. *Visual Neurosci.* **9**, 243–251 (1992).
47. Westheimer, G. Visual-Acuity and Hyper-Acuity. *Inves. Ophthalmol. Vis. Sci.* **14**, 570–572 (1975).
48. Lee, B. B., Wehrhahn, C., Westheimer, G. & Kremers, J. Macaque ganglion cell responses to stimuli that elicit hyperacuity in man: detection of small displacements. *J. Neurosci.* **13**, 1001–1009 (1993).
49. Dhruv, N. T., Tailby, C., Sokol, S. H., Majaj, N. J. & Lennie, P. Nonlinear signal summation in magnocellular neurons of the macaque lateral geniculate nucleus. *J. Neurophysiol.* **102**, 1921–1929 (2009).
50. Schwartz, G. W. *et al.* The spatial structure of a nonlinear receptive field. *Nat. Neurosci.* **15**, 1572–1580 (2012).
51. Huberman, A. D. & Niell, C. M. What can mice tell us about how vision works? *Trends Neurosci.* **34**, 464–473 (2011).
52. Kuhlman, S. J., Tring, E. & Trachtenberg, J. T. Fast-spiking interneurons have an initial orientation bias that is lost with vision. *Nat. Neurosci.* **14**, 1121–1123 (2011).
53. Ko, H. *et al.* The emergence of functional microcircuits in visual cortex. *Nature* **496**, 96–100 (2013).
54. Wiesel, T. N. & Hubel, D. H. Ordered arrangement of orientation columns in monkeys lacking visual experience. *J. Comp. Neurol.* **158**, 307–318 (1974).
55. Yang, G., Pan, F., Parkhurst, C. N., Grutzendler, J. & Gan, W. B. Thinned-skull cranial window technique for long-term imaging of the cortex in live mice. *Nat. Protoc.* **5**, 201–208 (2010).
56. Pelli, D. G. The VideoToolbox software for visual psychophysics: Transforming numbers into movies. *Spatial Vision* **10**, 437–442 (1997).
57. Brainard, D. H. The Psychophysics Toolbox. *Spat. Vis.* **10**, 433–436 (1997).
58. An, X. *et al.* Distinct functional organizations for processing different motion signals in V1, V2, and V4 of macaque. *J. Neurosci.* **32**, 13363–13379 (2012).
59. Pan, Y. *et al.* Equivalent representation of real and illusory contours in macaque V4. *J. Neurosci.* **32**, 6760–6770 (2012).
60. An, X., Gong, H., McLoughlin, N., Yang, Y. & Wang, W. The mechanism for processing random-dot motion at various speeds in early visual cortices. *PLoS one* **9**, e93115 (2014).
61. Van den Bergh, G., Zhang, B., Arckens, L. & Chino, Y. M. Receptive-field Properties of V1 and V2 Neurons in Mice and Macaque Monkeys. *J. Comp. Neurol.* **518**, 2051–2070 (2010).

Acknowledgments

This work was supported by National '973' Programmes 2009CB941303 and 2011CBA00400, the National Natural Science Foundation of China (Nos. 31371112). The funders had no role in study design, data collection and analysis, decision to publish, or preparation of the manuscript. We thank Drs. Nigel Daw, Michael Stryker, Yifeng Zhang, Jianzhong Jin, Ian Andolina and Niall McLoughlin for comments and suggestions on the data analysis and manuscript writing.

Author contributions

X.Z. and Y.Y. conceptualized the research idea and designed the experiments. X.Z., H.L., J.P. and S.C. collected the data. X.Z., X.A., W.W. and Y.Y. did the data analysis. X.Z., X.A., D.L., W.W. and Y.Y. wrote the manuscript.

Additional information

Supplementary information accompanies this paper at <http://www.nature.com/scientificreports>

Competing financial interests: The authors declare no competing financial interests.

How to cite this article: Zhang, X. *et al.* The Topographical Arrangement of Cutoff Spatial Frequencies across Lower and Upper Visual Fields in Mouse V1. *Sci. Rep.* **5**, 7734; DOI:10.1038/srep07734 (2015).



This work is licensed under a Creative Commons Attribution-NonCommercial-NoDerivs 4.0 International License. The images or other third party material in this article are included in the article's Creative Commons license, unless indicated otherwise in the credit line; if the material is not included under the Creative Commons license, users will need to obtain permission from the license holder in order to reproduce the material. To view a copy of this license, visit <http://creativecommons.org/licenses/by-nc-nd/4.0/>